Benchmark Tests for Strong Ground Motion Prediction Methods using Theoretical Methods

Y. Hisada
School of Architecture, Kogakuin University, Tokyo, Japan

M. Nagano
Tokyo University of Science, Chiba, Japan

A. Nozu
The Port and Airport Research Institute, Kanagawa, Japan

K. Miyakoshi
Geo-Research Institute, Osaka, Japan

K. Asano
Disaster Prevention Research Institute, Kyoto University, Kyoto, Japan

T. Matsumoto
Shinozuka Research Institute, Tokyo, Japan

T. Nakagawa
Fujita Corporation, Tokyo, Japan

SUMMARY:
We performed benchmark tests of the three theoretical methods for simulating strong motions: the wavenumber integration method, the discrete wavenumber method, and the thin layer method. We investigate the applicability of the methods through 6 Steps considering wide range of frequencies and hypocentral distances under the same source, path and site condition. We started from simple point sources in simple media in Step1, and extended sources in Step 2. Then, we used more complicated and realistic source and media models in Steps 3 and 4. Finally, we tested actual sources in the Kanto sedimentary basin, such as the 1923 Kanto earthquake (M7.9) in Steps 5 and 6. We obtained excellent agreements in almost all the cases, but found considerable discrepancies under certain conditions, such as the cases for large epicentral distances in the media of different formulations of Q (the quality factor), and the different approximations of surface sources.

Keywords: Benchmark Test, Strong Ground Motion Predication, Theoretical Methods

1. INTRODUCTION

Recently, various methods for predicting strong ground motions have been applied to engineering purposes, such as the safety evaluations of high-rise buildings and nuclear power plants, and the damage estimations of cities for large hypothesical earthquakes. Nonetheless engineers tend to be sceptical about the reliability of the predicted results, because they occasionally show large discrepancies using different methods, even under the same source, path, and site conditions. To investigate the causes of those discrepancies, we have carried out a series of benchmark tests since 2009, using the three-types of major methods for predicting strong ground motions; they are the theoretical, numerical, and stochastic methods.

In this paper, we describe the results of the benchmark tests of the theoretical methods. Those of the numerical and stochastic methods are presented in the subsequent papers (Yoshimura et.al., 2012; Kato et.al, 2012 in this volume). Even though the theoretical methods have limited applicatiosn to flat layered media, they are one of the most useful tools for simulating strong motions, because of the high accuracies, the broad frequency band, and the short computing time. On the other hand, there are numerous theoretical methods based on different formulation and coding. Thus, we have conducted

the benchmark tests using the three representative methods: the wavenumber integration, the discrete wavenumber, and the thin layer methods (e.g., Hisada, 1995; Bouchon, 1981; Nagano *et.al*, 2007).

The benchmark tests consist of 6 steps. We started from very simple point and extended sources in simple media in Steps 1 and 2. Then, we tested more complicated and realistic sources and media in Steps 3 and 4. Finally, we applied them to actual source models, including the 1923 Kanto earthquake (M7.9), in the Kanto sedimentary basin in the Steps 5 and 6.

2. BENCHMARK TESTS OF THEORETICAL METHODS

2.1. The Participants and Methods

Five groups of researchers/engineers participated in the tests using their own methods/codes. **Table 1** shows the participants and methods. The wavenumber integration method by Hisada & Matsumoto and Nakagawa (Hisada, 1995), and the discrete wavenumber method by Nozu (2002) and Miyakoshi & Asano (Bouchon, 1981) are theoretically similar method on the basis of the wavenumber integration, but the numerical integration schemes are different. The former uses general numerical integration techniques, such as the Simpson and Filon formulas for smaller and larger wavenumbers, respectively, whereas the latter uses the technique similar to the FFT algorism. As for the propagator matrix, all the methods use the R/T (Reflection/Transmission) matrix methods, which are numerically stable up to very high frequencies. On the other hand, the thin layer method by Nagano (2007) combines the theoretical and numerical wavefields in the horizontal and vertical directions, respectively. It uses the discretization technique of the Galerkin method along the vertical direction, and superposes the eigen modes to obtain ground motions. Even though it has to assume a rigid basement to compute the eigen modes, the computing time is generally very short. On the other hand, a viscoelastic boundary and a highly damping buffer zone are introduced to reduce the artificial reflections from the basement, especially at the stations of large distances.

The one of the biggest differences among the participants is the formulation of Q (quality factor). Through the tests, we asked the participants to use the frequency dependent Q, as shown in **Tables 4. 7, and 9**. The most participants introduce Q in the imaginary parts of Vs and Vp, using the following equation.

$$V^* = V\left(1-\frac{i}{2Q}\right)^{-1} \approx V\left(1+\frac{i}{2Q}\right) \qquad (1)$$

This formulation is simple, but is does not satisfy the causality condition. On the other hand, Miyakoshi & Asano use the following formula (Aki and Richards, 1981),

$$V^* = V\left(1-\frac{1}{\pi Q}\ln\frac{\omega_{REF}}{\omega}-\frac{i}{2Q}\right)^{-1} \approx V\left(1+\frac{1}{\pi Q}\ln\frac{\omega}{\omega_{REF}}+\frac{i}{2Q}\right) \qquad (2).$$

where, ω_{REF} is the reference circular frequency. On the contrary to equation (1), this formula satisfies the causality condition, but Q is independent of frequencies (constant Q), and we have to set a certain value for ω_{REF}. In addition, the values of medium velocities are frequency dependent (see **Figure 6**), which introduces the dispersion in waveforms.

Table 1. Participants and methods (○: Fully participating, △: Partially participating, ×: Not participating)

No	Participant	Method	Code	Step1	Step2	Step3	Step4	Step5	Step6
1	Hisada & Matsumoto	Wavenumber Integration Method	Hisada	○	○	○	○	○	○
2	Nagano	Thin Layer Method	Nagano	○	○	○	○	○	○
3	Nozu	Discrete Wavenumber Method	Nozu	○	○	△	×	○	×
4	Miyakoshi & Asano	Discrete Wavenumber Method	O.Coutant*	○	○	△	×	○	○
5	Nakagawa	Wavenumber Integration Method	Hisada	○	○	○	○	×	×

Note *: Dr. O.Coutant coded the original program based on Bouchon (1981), and Prof. Asano modified it.

2.2. Steps 1 and 2

Tables 2 & 3, and **Figures 1 & 2** show the models of Steps 1 and 2, respectively. Those simple starting models are basically same as those of Day *et.al.*(2000, 2003). Step 1 consists of 4 models (T11 to T14), by considering a point source of 2 or 20 km depths, and the 2 different media (homogeneous bedrock, or two-layered half-spaces), whose material properties are shown in **Table 4**. As shown in **Figure 1**, we locate the point source along the Z axis, and compute ground motions at the 6 stations from 2 km to 100 km of the epicentral distances. The source model is a point source of strike slip (strike=0 deg, dip=90 deg, rake=0, deg, $M_0=10^{18}$ Nm), and its moment rate function is the exponential-type,

$$\dot{M}(t) = M_0 \cdot \frac{t}{T^2} \cdot e^{-\frac{t}{T}} \qquad (3)$$

where, we use T = 0.1 s. **Figure 3** shows the moment, moment-rate functions, and the Fourier amplitude spectrum of the moment-rate function.

On the other hand, Step 2 consists of 2 models of extended source models. T21 is the lateral slip fault model, as shown in **Figure 2** (strike=90 deg, dip=90 deg, rake=180, deg, L=8 km, W=4 km). The shallowest edge of the faults is at located 2 km depth, and the hypocenter is at 4 km depth along the Z axis. The rupture front is continuous using Vr = 3 km/s. The slip functions (D = 1 m) has the same shape as those of **Figure 3**. T22 is the inverse slip fault model (see the detail in Day *et.al* (2000)).

Table 2. Model lists of Step 1

Model	T11	T12	T13	T14
Media	Bedrock	2 Layers Model		
Q	Infinite (No Damping)		Table 1	Infinite
Source Depth	2 km			20 km
Frequencies	0 - 20 Hz			
Output	6 points (+002, +006, +010, +030, +050, +100 km)			
Reference	UHS.1[4)]	LOH.1[4)]	LOH.3[4)]	LOH.1[4)]

Table 3. Model lists of Step 2

Model	T21	T22
Media	2 Layers Model	
Q	Infinite (No Damping)	
Source Model	Lateral Slip Fault	Inverse Slip Fault
Frequencies	0 - 5 Hz	
Output	12 points (±002, ±006, ±010, ±030, ±050, ±100 km)	
Reference	LOH.2[4)]	LOH.4[4)]

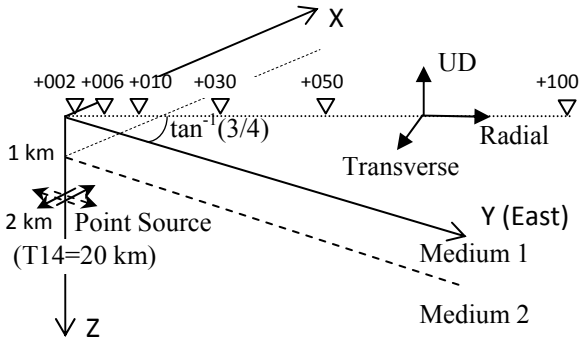

Figure 1. The point source and observation station for Step 1

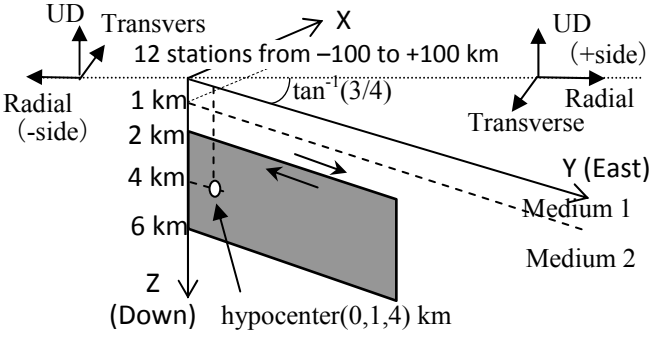

Figure 2. The fault model and station for T21

Table 4. Material properties of media for Steps 1 and 2

Layer	Thickness (m)	Vp (m/s)	Vs (m/s)	Density (kg/m^3)	Qp=Qs
Sediment	1,000	4,000	2,000	2,600	40f
Bedrock	–	6,000	3,464	2,700	70f

Note 1: f of Q stands for frequency (Hz)
Note 2: the Bedrock model is the homogenous half- space

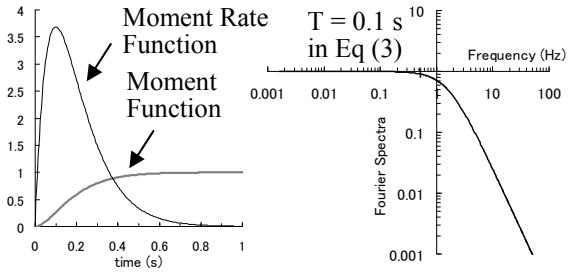

Figure 3. Moment, and moment-rate functions, and the Fourier amplitude spectra for Step 1

Since the amount of results is very large, and almost all the results show very good agreements, we only show the selected results, especially showing the distinct differences. **Figure 4** shows the comparisons of the three components of velocities at the 100 km distance using the T11 model. The

numbers in the waves indicate the maximum/minimum values of amplitudes. As shown in **Figure 4(a)**, the waves by the 4 researchers are practically identical (Nakagawa's results are not listed, because of the use of Hisada's code). However, when we look at the close up waves as shown in **Figure 4(b)**, we see small differences. One of them is the different peak values, which caused by the rough time interval (0.01 s), as compared with sharp peak with very short duration (see **Figure 3**). The other noises appear in the later phases in Nozu's results, which come from the artificial adjacent domains; they are introduced by the formulation of the discrete wavenumber method.

Figure 5 shows the comparisons of the three components of velocities at the 100 km distance using the T13 model. The top three waves are almost identical, which used Q of **Table 4** based on equation (1), whereas the bottom waves are different from the others. This is caused by the use of the constant Q based on equation (2), where $\omega_{REF} = 1$ (rad/s; f_{REF} (the reference frequency) $\fallingdotseq$ 0.16 Hz).

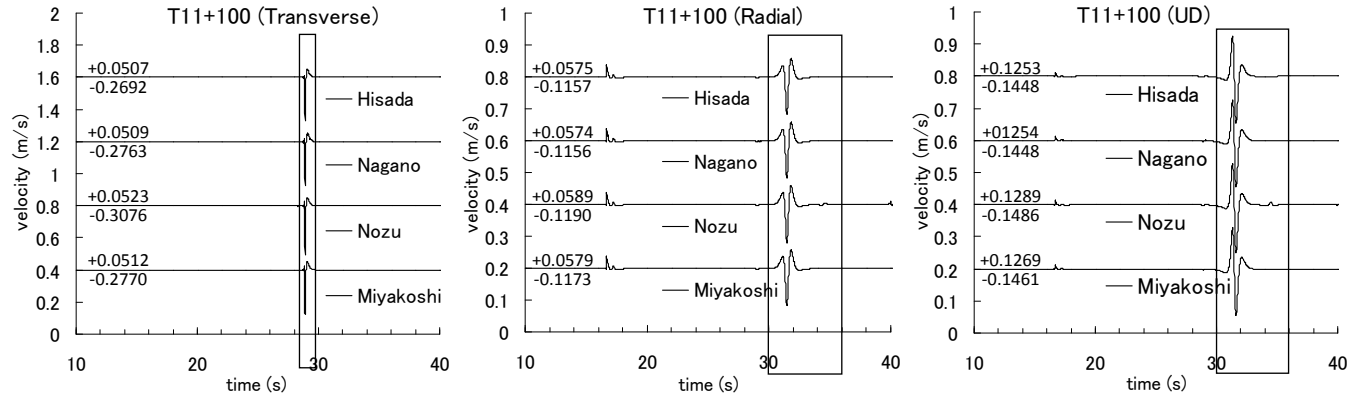

(a) Full waveforms of velocities (the values are the maximum/minimum values of amplitudes)

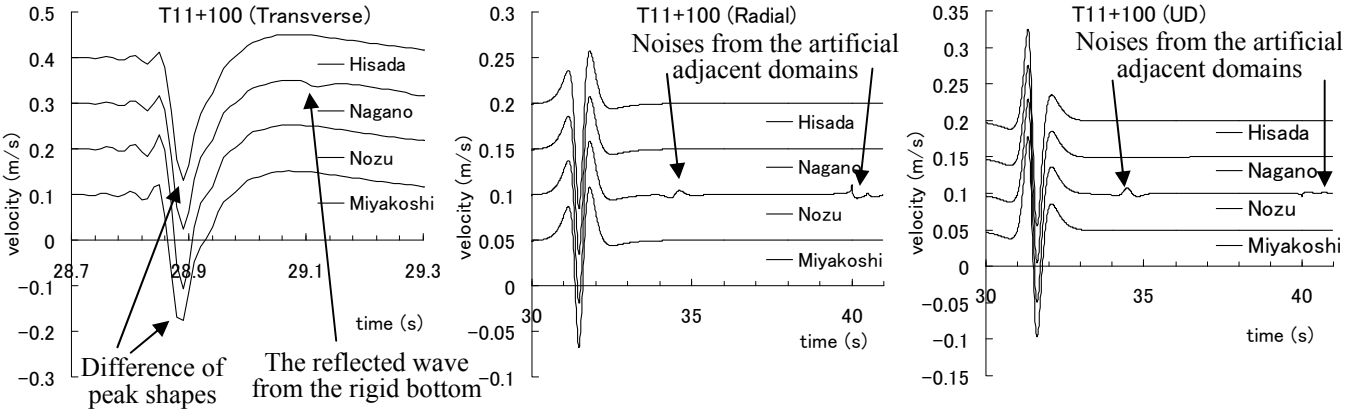

(b) Close up of velocity waveforms (the close up areas are indicated in the boxes in Figure 4(a))

Figure 4. Comparisons of the three components of velocities at the 100 km distance using the T11 model

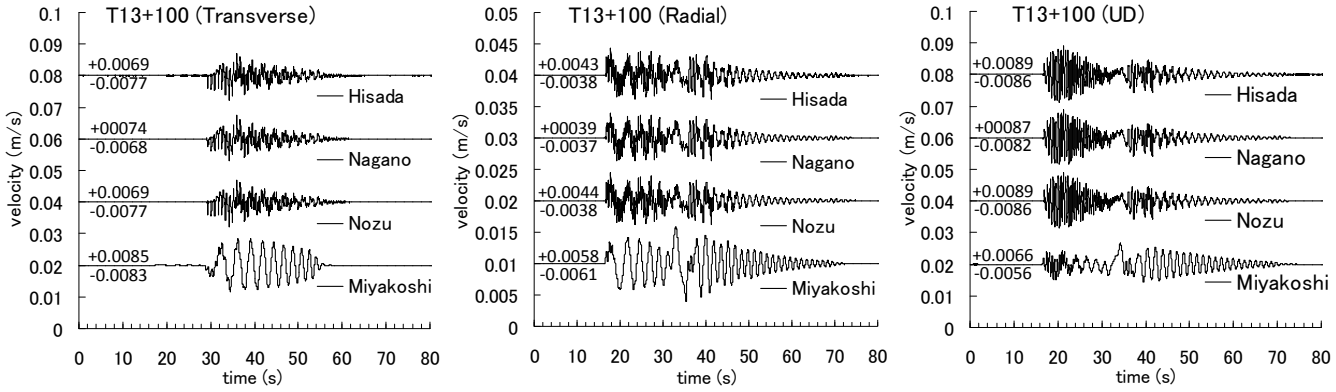

Figure 5. Comparisons of the three components of velocities at the 100 km distance using the T13 model

It is interesting to check the effects of the different constant Q based on equations (1) and (2). **Figure 6** shows frequency vs. normalized medium velocities using different f_{REF} (=0.1, 1.0 and 10 Hz) in equation (2). The figure shows the dispersive characteristics; the velocities keep the original values at $f=f_{REF}$, but varies from about -5% at 0.01 Hz to about + 5% at 100 Hz.

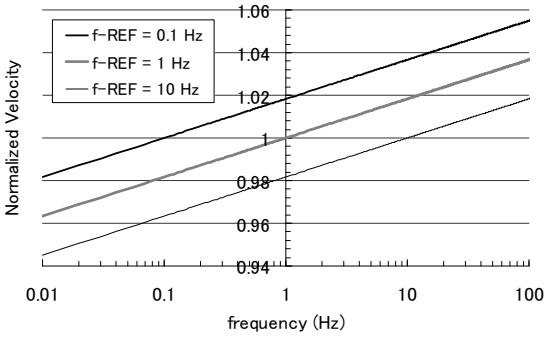

Figure 6. Frequency vs. normalized medium velocities using different f_{REF} based on Eq (2)

Figure 7 shows the comparisons of the radial components of velocities at 100 km using the different constant Q (=40) for T13. In **Fig.7(left)**, the top is the velocity of eq. (1), and the next two are the velocities of eq. (2) using f_{REF} = 1.0 and 0.16 Hz, respectively. Those waves are computed by Hisada's code, and the bottom is Miyakoshi's result using f_{REF} = 0.16 Hz;. The last two waves are almost identical. **Fig.7(center) & (right)** are close ups of the initial and coda parts. In the initial parts, the wave of eq. (1) starts before signal's arrival; it does not satisfy the causality condition. On the contrary, the waves of eq. (2) show the sharp rises just after signal's arrivals. However, the arrival times are different between f_{REF} = 1.0 and 0.16 Hz. The former is slower, but close to the wave of eq. (1). On the other hand, we see completely different phases in the coda parts in **Fig.7 (right)**. Since the waves of eq. (1) and those of eq. (2) using f_{REF} =1.0 Hz show similar phases,. f_{REF} =1.0 Hz in eq. (2) seems the one of the best choice in this particular case.

Figure 8 shows the comparisons of the velocities at 100 km using the T14 model. All the waves except Nagano (the thin layer method) are almost identical. Nagano's results are smaller than the other, because it computed only up to 7 Hz, but not 25 Hz. The thin layer method is very accurate and efficient for shallow sources at close distance, but may not be efficient for deep sources at long distances at very high frequencies.

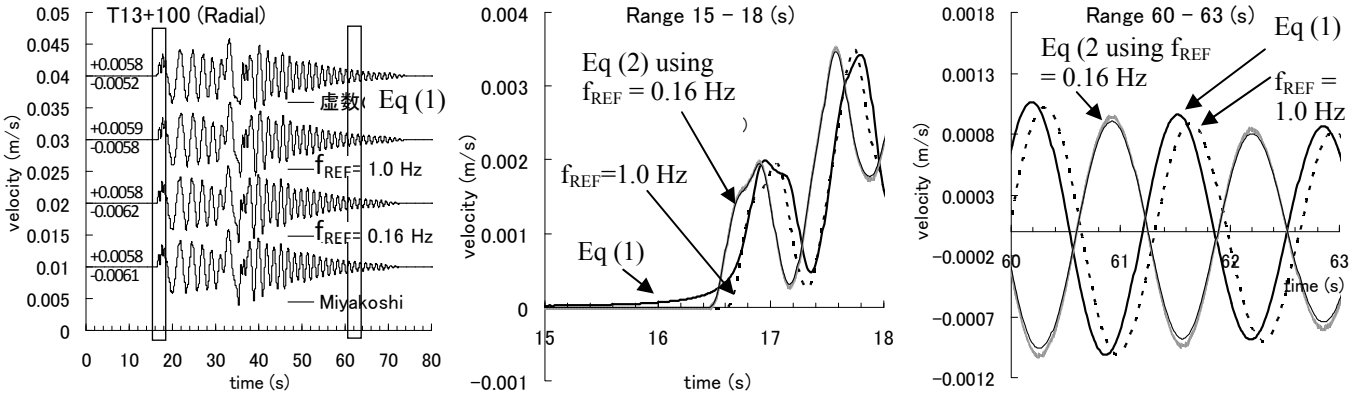

Figure 7. Comparisons of the radial velocities at 100 km using the T13 model and the different constant Q=40

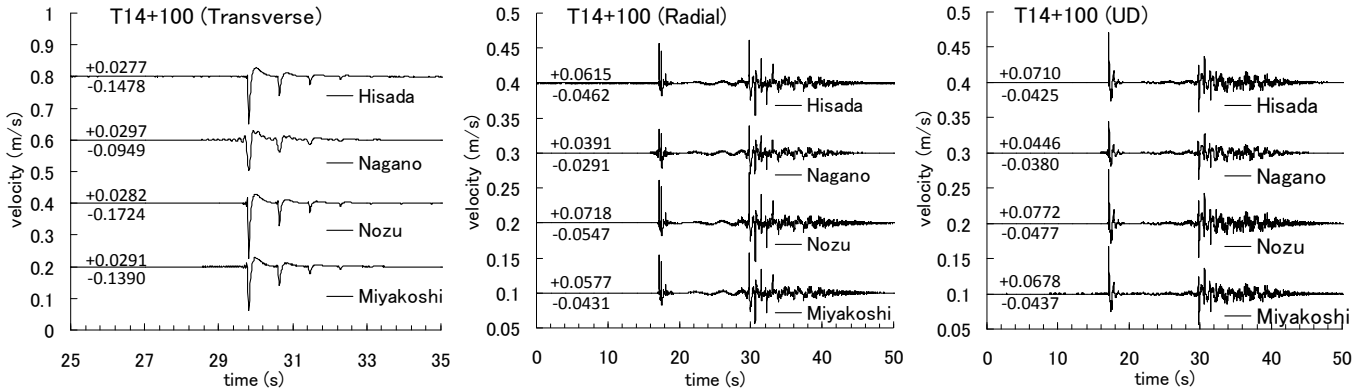

Figure 8. Comparisons of the three components of velocities at 100 km using the T14 model

2.2. Steps 3 and 4

Tables 5 and 6 show the model lists of Steps 3 and 4, respectively, which are more complicated and realistic for sources and media than those of Steps 1 and 2. We use the 4 layered model shown in **Table 7**, and the 2 layered model same as **Table 4**. We use point sources in Step 3 with 2 km and 0 km depths. The source parameters are the same as those of Step 1, except the moment-rate function. We use the following the Gaussian-type function,

$$\dot{M}(t) = M_0 \cdot \frac{1}{\sqrt{2\pi}\sigma} \cdot \exp\left(-\frac{(t-\mu)^2}{2\sigma^2}\right) \qquad (4)$$

where, σ is the standard deviation, and μ is the peak time. We use σ=0.2 (s) and μ=0.8 (s), which are the same as those of Day *et.al.* (2000).

On the other hand, we use the 4 models of the lateral slip fault in Step 4, where the basic source parameters are the same as T21, except the slip function. We use the pseudo-dynamic slip function (Nakamura and Miyatake, 2000), as shown in **Figure 9**, using F_{max}=6 Hz, td≒0.05305 s, tr≒0.6667 s, ts=1.0 s, and V_m≒5.168 m/s. Among 4 models (T41-T44), the first three are the buried models same as Step 2 (see **Figure 2**), and the last model is the surface fault, whose top edge reaches the free surface. We also introduce three different rupture models using Vr= 3 km/s. T41 and T42 assume the discrete ruptures at the intervals of 1 km^2. The former uses the constant Vr, whereas the latter uses random values in the rupture times, using the following equation,

$$t_{ij} = \frac{\eta_{ij}}{Vr} + \varepsilon_{ij} \quad (\ w/2Vr > \varepsilon_{ij} > -w/2Vr\ ) \qquad (5)$$

where, η_{ij} is the distance between the hypocenter and the centres of sub-faults, *w* is the size of the sub-faults, and ε_{ij} is the random numbers. We generate three sets of the random numbers. On the other hand, we assume the continuous rupture fronts using constant Vr in T41 and T42.

Table 5. Model lists ofr Step 3

Model	T31	T32	T33
Media	4 Layers Model		2 Layeres Model
Q	Infinite	Table 7	
Source Depth	2 km (Buried)		0 km (Suface)
Frequencies	0 - 5 Hz		
Output	6 points (+002, +006, +010, +030, +050, +100 km)		

Table 6. Model lists of Step 4

Model	T41	T42	T41	T42
Media	2 Layers Model			
Q	Table 4			Infinite
Fault Model	Lateral Slip Fault (Buried)			(Surface)
	1 km^2 (constant)	1 km^2 (random)	continunous	
Frequencies	0 - 5 Hz			
Output	12 points (±002, ±006, ±010, ±030, ±050, ±100 km)			
	1 sets	3 sets	1 sets	

Table 7. Material properties of the 4 layered model

No	Thickness (m)	Vp (m/s)	Vs (m/s)	Density (kg/m^3)	Qp=Qs
1	200	1,600	400	2,000	20f
2	400	2,600	1,000	2,400	30f
3	1,000	4,000	2,000	2,600	40f
4	∞	6,000	3,464	2,700	70f

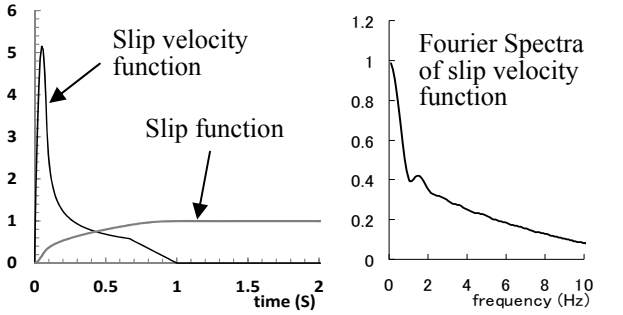

Figure 9. The pseudo-dynamic slip and velocity functions

Again, the amount of results is large, and almost all the comparisons show exellent agreements. Thus, we only show the results showing the distinct differences. **Figure 10** shows the comparisons of the radial components of velocities at the 10 km distance using T31. The waves seem almost identical each other, whereas **Figure 10 (b) and (c)** show the close up of the initial (0-5 s) and the coda waves (30-35 s). Even though the amplitudes are very small, we see the base line drifts except Nagano' results. Those permanent drifts are probably caused by the use of the unphysical frequency dependent Q. Q becomes 0 (i.e., infinite damping), when f goes to 0 Hz. The thin layer method by Nagano did not show these drifts, because those low frequency noises are probably absorbed tin the damping

buffer zone at the bottom.

Figure 11 shows the comparisons of velocities at the 100 km distance using T33 (a surface point source). The results between Hisada and Nagano are almost identical, but those of Miyakoshi and Nakagawa are small. Those small amplitudes are caused by the approximated depth (50 m). This approximation was needed for carrying out the numerical wavenumber integration; in the case of the same depths of the source and observation points, the convergences of integrants are extremely slow for increasing wavenumbers. On the contrary, the methods by Hisada and Nagano eliminated those problems, theoretically (see Hisada, 1995; Nagano and Watanabe, 2007).

Figures 12 and 13 show the comparisons of velocities and their Fourier amplitudes at 10 km using the T41, T42, and T43 models. T41 and T42 use the discrete rupture processes at the intervals of 1km^2, with the constant and random rupture times, respectively. T42 use three sets of random numbers. On the other hand, T43 use the continuous rupture considering very small sizes of sub-faults, which caused very small amplitudes at higher frequencies. The discrepancies of the results among three researchers are very small for T41 and T43. On the other hand, those of T42 show random characteristics, but not very large differences. It is noted that the Fourier amplitudes of T41 shows the sharp peaks around 3 Hz, whereas those of T42 are not clear. Those peaks are caused by the artificial rupture interval times between adjacent sub-faults (Vr/w=3/1= 3 Hz).

Figure 14 shows the comparisons of the displacements at 2 km using T44. The displacements are computed by integrating velocities in the time domain. Since the site is very close to the surface fault, we see the fling steps (the permanent offsets with large amplitudes). Beside the benchmark tests, we also computed the static terms, which are the convolution of the slip function and static Green's function (Hisada and Bielak, 2003). The results by three researchers are almost identical, and the values of the permanent offsets agree with the static values. While those values were computed by no damping (Q) media, the displacements showing "Including Q of Eq (2)" in **Fig.14** are the results using the frequency dependent Q. Their amplitudes are increasing or decreasing in time, and do not show the correct values. This is probably caused by the unphysical Q, that is, the value becomes 0 (infinite damping), when frequency goes to 0 Hz

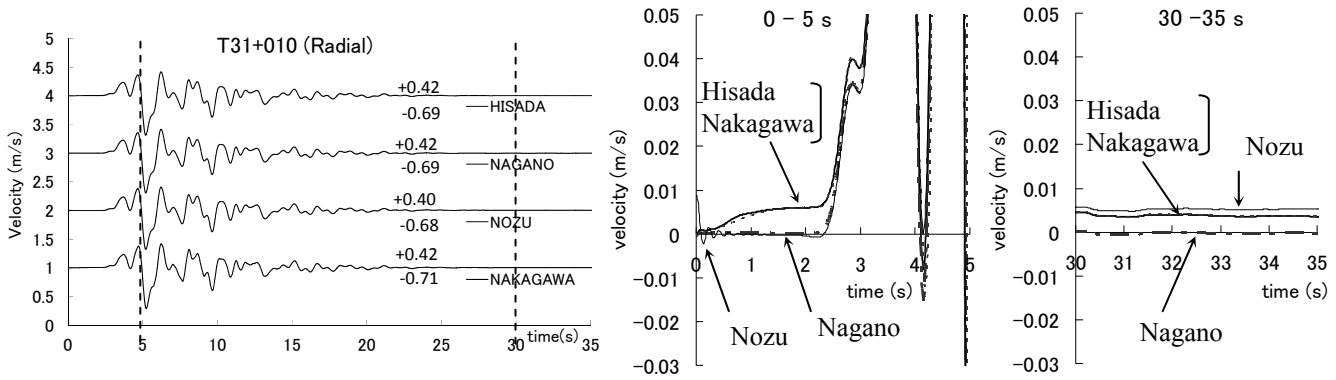

(a) Whole wave forms (b) Close up between 0 to 5 s (c) Close up between 30 -35 s

Figure 10. Comparisons of the radial components of velocities at the 10 km distance using the T31 model

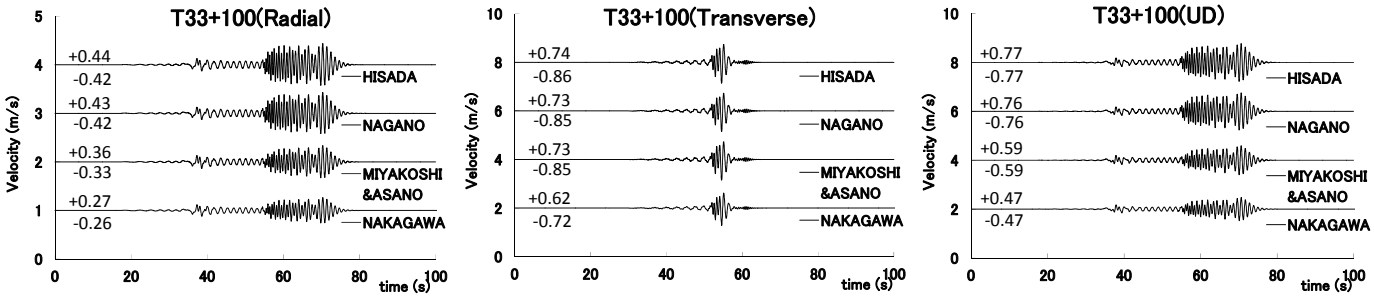

Figure 11. Comparisons of the three components of velocities at the 100 km distance using the T33 model

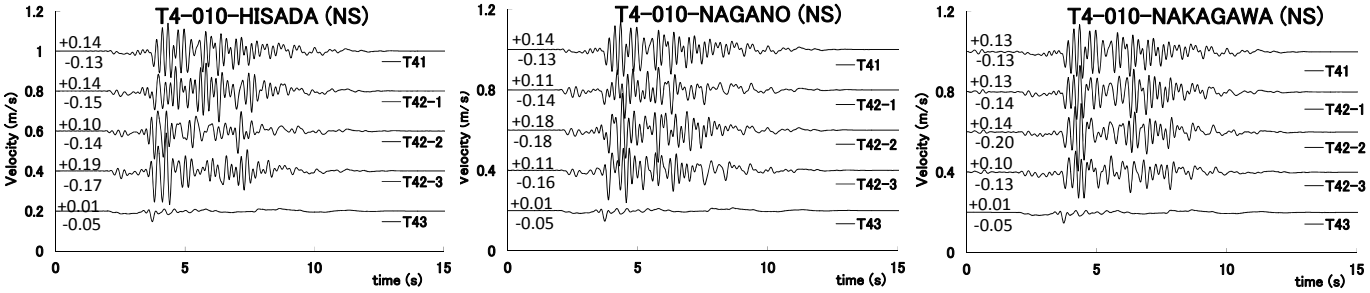

Figure 12. Comparisons of velocities at the 10 km distance using the T41, T42, and T43 models

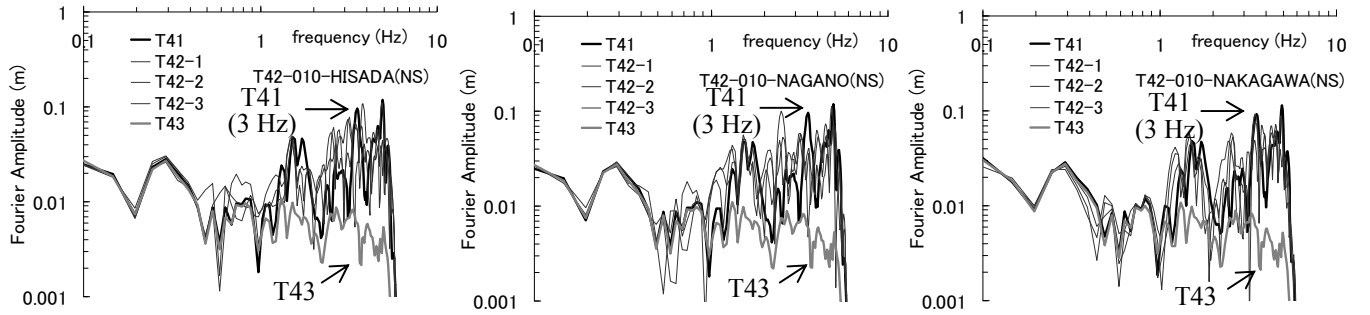

Figure 13. Comparisons of the Fourier amplitudes at the 10 km distance using the T41, T42, and T43 models

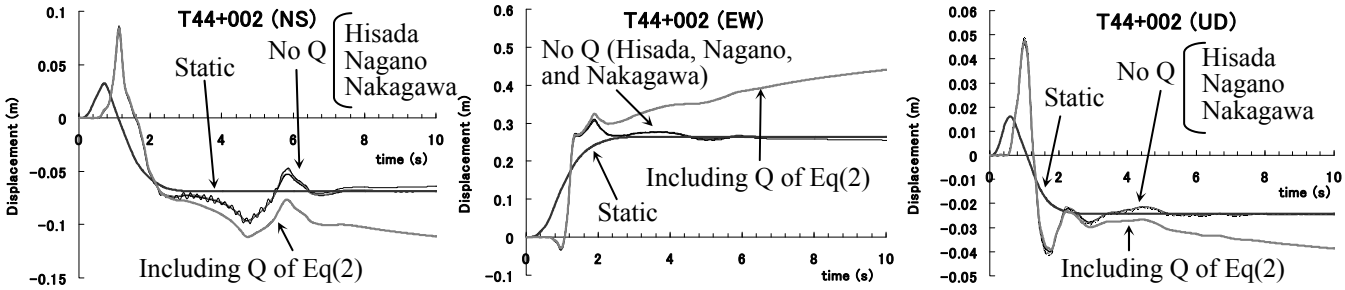

Figure 14. Comparisons of the tree components of displacements at the 2 km distance using the T44 model

2.4. Steps 5 and 6

Table 8 shows the model lists of Steps 5 and 6, where we use the actual source models in the Kanto sedimentary basin. In Step 5, we use relatively small earthquakes, and compare the simulated waves and observation records. As an example, **Table 9** and **Figure 15** show the source parameters and the locations of the the 1990 West Kanagawa earthquake (the Odawara earthquake in Sato *et.al.*, 1998), together with the observation stations. In Step 6, we simulate long-period ground motions of the 1923 Great Kanto earthquake. **Table 10** and **Figure 16** show the source parameters and the location of the fault (see for more detail in Sato *et.al.*, 2005)

Table 9 shows the material properties and the locations of the top boundaries of the layers of the Kanto basin model. Although the original data are for the 3-D basin model (The headquarters for Earthquake Research Promotion, 2009), we use the values just under the observation stations as the flat layered models. The table shows examples of the boundary depths at the four sites.

Figure 17 shows the comparisons of the NS components of velocities for the 1990 West Kanagawa earthquake at the KNO, ASK, JSK, and FUT sites. The top waves are observed records (AIJ, 1996), and the next three waves are the simulations by three researchers. The excellent agreements are obtained among the simulations. The simulations at KNO, which is located at the rock site closest to the epicenter, show excellent agreements with the records. However, the other results do not agree

well with the records, especially the surface waves excited in the Kanto basin. These results clearly indicate the limitations of the theoretical methods based on the flat layered structures.

Table 8. Model lists of Steps 5 and 6

Model	Step 5			Step 6
	T51	T52	T53	T61
Earthquake	1990 West Kanagawa EQ (Mj 5.1)	1990 Near Izu-Oshima EQ (Mj 6.5)	1992 Tokyo Bay EQ (Mj 5.7)	1923 Great Kanto EQ (Mj 7.9)
Source Model (Reference)	Point （Sato, T. et al. 1998 ）	Extended （Yamada and Yamanaka, 2003)	Point （Yamada and Yamanaka, 2003)	Extended （Sato, H., et. al., 2005)
Media	Flat layered half-spaces at the observation stations using the 3D Kanto basin model			
Q	Table 9			
Frequencies	0～0.33 Hz			
Output	19 sites in the Kanso basin, where the strong motion data are available (AIJ, 1996)			

Table 9. The source parameters of the 1990 West Kanagawa EQ

Longitude of Epicenter （°）	35.2133
Latitude of Epicenter （°）	139.0998
Depth of Epicenter (km)	15.3
Strike Angle （°）	215
Dip Angle （°）	35
Rake Angle （°）	40
Sesmic Moment （Nm）	3.3×10^{16}

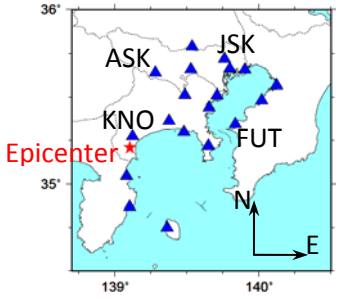

Figure 15. Locations of the epicenter of the 1990 West Kanagawa EQ and observation stations

Table 10. The source parameters of the 1923 Great Kanto EQ

Fault Length （km）	130
Fault Width （km）	70
Longitude of Epicenter （°）	35.3847
Latitude of Epicenter （°）	139.1144
Depth of Epicenter (km)	10.651
Strike Angle （°）	294
Dip Angle （°）	16
Rupture Velocity （km/s）	3
Sesmic Moment （Nm）	9.94×10^{20}

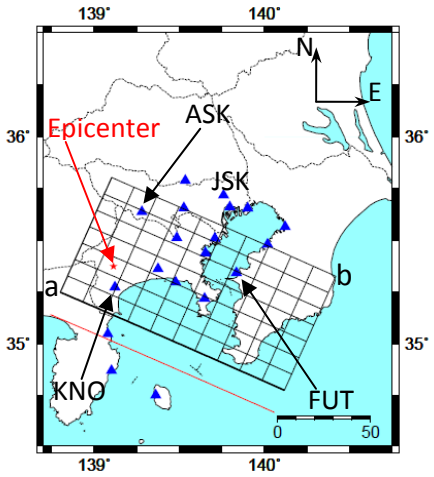

Figure 16. Locations of the fault and epicenter of the 1923 Great Kanto EQ and observation stations

Table 11. The material properties and the depths of the top boundaries of the Kanto basin model

No.	ρ	Vp	Vs	Qp=Qs	Depth of Top Boundary （m）			
	(kg/m^3)	(m/s)	(m/s)		Kuno (KNO)	Asakawa (ASK)	Hongo (JSK)	Futtsu(FUT)
1	1,950	1,800	500	500f*	0	0	0	0
2	2,050	2,100	700	700f	—	—	—	—
3	2,100	2,300	900	900f	152	6	406	260
4	2,150	2,400	1,000	1000f	—	—	—	—
5	2,250	3,000	1,500	1500f	384	51	1,736	1,426
6	2,300	3,200	1,700	1700f	—	—	—	—
7	2,450	4,200	2,400	2000f	616	—	—	—
8	2,600	5,000	2,900	2000f	676	—	—	—
9	2,650	5,500	3,200	2000f	1,317	201	3,067	3,347
10	2,700	6,000	3,530	2000f	1,798	7,107	7,830	6,792
11	2,800	6,700	3,940	2000f	4,494	17,768	19,575	16,980

Finally, **Figure 18** shows the comparisons of the NS components of velocities for the 1923 Great Kanto earthquake at the KNO, ASK, JSK, and FUT sites. Even though the source model and the media are very complicated, the excellent agreements are obtained among the researchers. This clearly shows the reliability of the theoretical methods under the same source, path and site conditions.

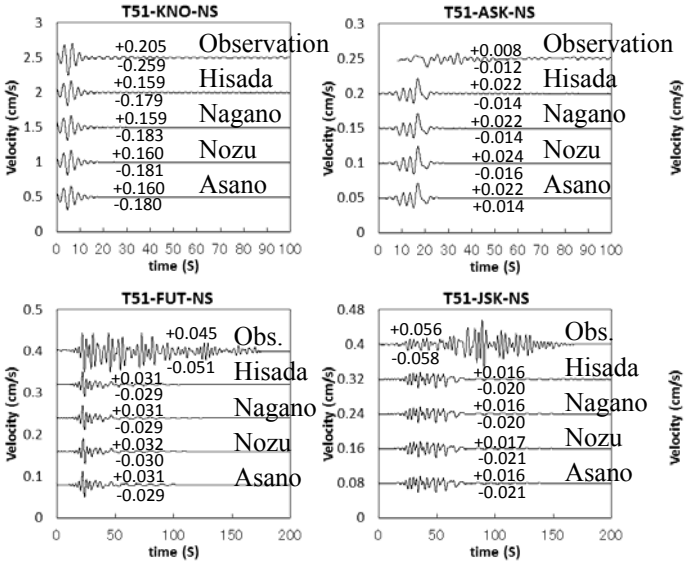

Figure 17. Comparisons of velocities for the 1990 West Kanagawa earthquake (NS components)

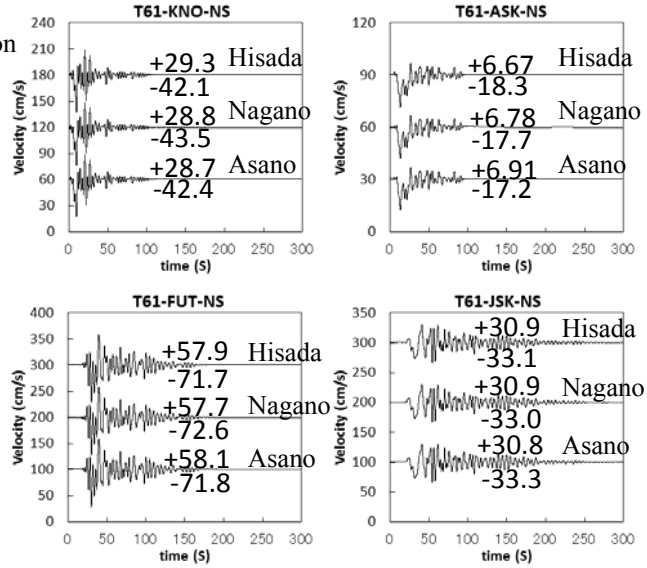

Figure 18. Comparisons of velocities for the 1923 Great Kanto earthquake (NS components)

3. CONCLUSIONS

We performed benchmark tests of 6 Steps, using the three different theoretical methods, and obtained excellent agreements in almost all the results. At the same time, we found discrepancies, such as the cases for large epicentral distances in the media with different formulations of Q (medium damping), and the different approximations of surface sources.

AKCNOWLEDGEMENT

This work was supported by Grant-in-Aid for Scientific Research (B) of MEXT (Japan Ministry of Education, Culture, Sports, Science and Technology), and Research Centre of Urban Disaster Mitigation (UDM) in Kogakuin University. We also thank Prof. N. Yamada of Fukuoka University of Education, and Prof. R. Kobayashi of Kagoshima University for providing their source parameters, and Sub-Committee on Strong Motion Observation of Architectural Institute of Japan for providing the strong motion data.

REFERENCES

AIJ (Architectual Institute of Japan, 1996). Journal of architecture and building science, April.
Aki, K., and Richards, P. G. (1980). Quantitative seismology: Theory and methods, pp.167-185.
Bouchon, M.(1981). Bulletin of Seismological Society of America, Vol.71, pp.959-971.
Day, S. M. *et.al.* (2000). Final Report to PEER Center, Lifelines Program TASK 1A01, pp.1-24.
Day, S. M. *et.al.* (2003). Final Report to PEER Center, Lifelines Program TASK 1A02, pp.1-32.
Hisada, Y. (1995). Bulletin of Seismological Society of America, Vol.85, No.4, pp.1080-1093.
Hisada, Y. and Bielak, J. (2003). Bulletin of Seismological Society of America, Vol.93, No.3, pp.1154-1168,.
Nakamura, H. and Miyatake, T. (2000), Journal of the Seismological Society of Japan, Vol.53, No.1, pp.1-11.
Nagano, M. and Watanabe, T. (2007). AIJ Journal of Technology and Design, Vol.13, No.26, pp.451-456
Nozu, A. (2002). Technical Note of Port and Airport Research Institute, Japan, No.1037.
Sato, H. *et al.* (2005). Earthquake source fault beneath Tokyo, Science, Vol. 309, pp.462-464.
Sato, T. *et al.* (1998). Bulletin of Seismological Society of America, Vol.88, No.1, pp.183-205.
Yamada, N. and Yamanaka, H.. (2003), Journal of the Seismological Society of Japan, Vol.56, pp.111-123.